Carbohydrate Polymer Technologies and Applications 11 (2025) 100922

Contents lists available at ScienceDirect

Carbohydrate Polymer Technologies and Applications

journal homepage: www.sciencedirect.com/journal/carbohydrate-polymer-technologies-and-applications

Biopolymer beads composed of gamma-irradiated chitosan and dental-waste-derived alginate for dye removal applications

Prach Ponlawat [a], Narawadee Prathum [a], Pitchapa Pittayavinai [a], Ranida Tuanudom [a], Narudom Srisawang [a], Thongnard Kumchai [a], Phitchan Sricharoen [c], Ekasith Somsook [b], Titiya Meechai [a,*]

[a] Faculty of Dentistry, Bangkokthonburi University, Thawi Watthana, Bangkok 10170, Thailand
[b] NANOCAST Laboratory, Center for Catalysis Science and Technology (CAST), Department of Chemistry and Center of Excellence for Innovation in Chemistry, Faculty of Science, Mahidol University, 272 Rama VI Rd., Ratchathewi, Bangkok 10400, Thailand
[c] Division of Health, Cosmetic and Anti-Aging Technology, Faculty of Science and Technology, Rajamangala University of Technology Phra Nakhon, Bangkok, Thailand

ARTICLE INFO

Keywords:
Bio-beads
Gamma-irradiated chitosan
Alginate
Dental waste
Dye removal
Wastewater treatment
Adsorption
Degradation

ABSTRACT

This study presents the synthesis and characterization of bio-beads composed of gamma-irradiated chitosan and alginate derived from dental waste for the removal and degradation of Congo Red (CR) dye. Dental-grade alginate, typically used for impression-making, is repurposed as a sustainable matrix. The synthesized bio-beads were characterized using BEI, HRTEM, XRD, HAADF-STEM, EDS, FTIR, and BET analysis. UV–vis spectroscopy was used to evaluate dye removal efficiency. The gamma-irradiated chitosan coating enhanced surface area (68.045 m^2/g) and improved CR adsorption compared to non-irradiated chitosan. The gCS-AG beads exhibited excellent reusability, retaining over 80 % efficiency for 10 cycles. The synthesis is simple and eco-friendly, with irradiation improving chitosan solubility and surface binding. The study demonstrates the dual functionality of the beads in adsorption and partial dye degradation. Electrostatic interactions between protonated amine groups in chitosan and anionic sulfonate groups in CR play a dominant role in adsorption. Radical-induced cleavage of azo bonds under acidic conditions contributes to degradation. This work promotes waste valorization and green material development for wastewater treatment.

1. Introduction

Alginate, a hydrocolloid derived from brown seaweed, is extensively employed in dentistry for obtaining precise oral impressions, particularly for study models crucial in treatment planning and the fabrication of removable dentures. Its notable characteristics include exceptional detail capture of both teeth and gingival structures, alongside facile removal without inducing dimensional distortion. In this research, we focus on applying discarded alginate from clinical settings, specifically remnants deemed unsuitable for reuse in impression-taking processes. Such waste typically accumulates during the fabrication of removable dentures and the creation of dental study models. This study investigates the potential of these discarded alginate materials to be repurposed into bio-beads for dye adsorption in wastewater treatment applications. By leveraging these surplus materials, we aim to promote sustainable practices within the dental industry and mitigate waste, thereby contributing to improved environmental management in water treatment (Wu et al., 2012; Abourehab et al., 2022).

The research conducted by Vishwanathan et al. provides an in-depth analysis of the efficacy of chitosan and its derivatives in the remediation of heavy metals from aqueous effluents. The study demonstrates that chitosan exhibits a robust adsorption capacity for various toxic metals, including lead and cadmium (Vishwanathan et al., 2020). Further investigations by Puspaningrum et al. explored the effects of irradiation on chitosan, revealing that ionizing radiation modifies the polymer's structural properties, leading to an increased surface area that significantly enhances its adsorption efficiency for various contaminants. In parallel, the application of alginate, a polysaccharide derived from brown seaweed, in adsorbing pollutants, particularly dyes from industrial wastewater, has been extensively documented. Wang et al. highlighted alginate's effectiveness in sequestering dyes prevalent in the textile sector, underscoring its utility in mitigating water pollution

* Corresponding author.
E-mail address: titiya.mee@bkkthon.ac.th (T. Meechai).

https://doi.org/10.1016/j.carpta.2025.100922

Available online 27 June 2025

(Wang et al., 2017). Moreover, research by Bhattacharyya and Sharma quantified alginate's capability to remove organic pollutants and dyes from textile wastewater, reporting substantial dye removal efficiencies. Notably, alginate is recognized as a biocompatible and environmentally benign material, positioning it as a sustainable option for wastewater treatment applications.

The application of bio-beads synthesized from irradiated chitosan is pivotal to this research. Chitosan, a biopolymer extracted from the shells of crustaceans, exhibits superior adsorption capabilities for various contaminants, particularly heavy metals and organic compounds present in wastewater. In this study, chitosan will undergo controlled irradiation to augment its physicochemical properties, enhancing its efficacy in adsorbing toxins and dyes (Meechai et al., 2023). The irradiation process is designed to induce structural modifications in the chitosan, resulting in increased surface area and enhanced functional groups that facilitate stronger binding interactions with pollutants. The bio-beads produced by integrating gamma-irradiated chitosan with alginate derived from dental waste leverage the inherent adsorption properties of both constituents. This synergistic combination is expected to significantly enhance the system's efficacy in dye removal from wastewater. Moreover, this research addresses dual sustainability challenges: it innovatively utilizes dental industry byproducts while developing advanced wastewater treatment technologies (Mahmoodi et al., 2025). The resulting bio-beads promote more efficient pollutant uptake and align with environmentally sustainable practices, ultimately contributing to a reduction in dental waste and wastewater pollution. (Meechai et al., 2023; Coura et al., 2020; Areerob et al., 2022; Fathy et al., 2020; Tamer et al., 2022). This research aims to develop bio-beads composed of gamma-irradiated chitosan and alginate derived from dental waste, focusing on the practical and sustainable removal of dyes from wastewater (Keanjun et al., 2024). By utilizing natural materials and repurposing dental industry waste, this study offers a novel approach to wastewater treatment that addresses environmental concerns and contributes to the reduction of waste in the dental industry. Chitosan, derived from marine animals, has proven highly effective in adsorbing toxins such as heavy metals, while alginate, a natural polymer from seaweed, has shown promise in dye removal (Haririan & Asefnejad, 2024). The irradiation process further enhances the adsorptive properties of chitosan, increasing its surface area and improving its ability to bind with toxins. This innovative combination of materials aims to improve the efficiency of wastewater treatment while promoting the use of sustainable, environmentally friendly materials.

The use of natural polymers such as chitosan and alginate in dye adsorption has been extensively studied due to their availability, biocompatibility, and high affinity for pollutants. Chitosan, derived from chitin through deacetylation, possesses amino groups that can interact electrostatically with anionic dyes, such as Congo Red and Methyl Orange. Chitosan-based composites effectively removed various synthetic dyes from aqueous solutions, especially under acidic conditions. Similarly, Bhattacharyya and Sharma (2005) reported the significant adsorption capacity of chitosan for cationic and anionic dyes through surface complexation and hydrogen bonding (Bhattacharyya & Sharma, 2005). Alginate, a naturally occurring anionic polysaccharide extracted from brown algae, contains carboxyl and hydroxyl groups that allow strong binding with dye molecules and heavy metal ions (Koosha et al., 2025). Bhattacharyya and Sharma (2005) and Wang et al. (2018) confirmed its efficiency in removing dyes such as Rhodamine B and Congo Red, especially when used in hydrogel or bead form to enhance surface area and stability (Wang et al., 2018; Karthikeyan et al., 2005). Despite numerous studies on chitosan-alginate composites (Alavinia et al., 2023), the combination of gamma-irradiated chitosan and alginate derived from dental waste has not yet been explored for dye adsorption, representing a novel and sustainable approach.

2. Experimental

2.1. Materials

Dental waste product (Alginate), NaOH (98 %), were obtained from Merck, and Acetic acid, Tokyo Chemical Industry Co., Ltd. (TCI Chemicals). Sigma-Aldrich supplied $CaCl_2$ (≥99 %). Congo red dye was purchased from Acros Organic (Mumbai, India). Chitosan was irradiated with gamma rays at a sterilizing dose of 40 kGy, resulting in a molecular weight of 190 kDa and a degree of deacetylation of 95 %, and was provided by the Thailand Institute of Nuclear Technology (Public Organization) (Keanjun et al., 2024).

2.2. Apparatus

The X-ray diffraction (XRD) analysis was conducted using a Bruker D8 Advance A25 diffractometer equipped with a Ni filter (Cu K radiation: 0.154184 nm) and a one-dimensional multistrip detector (Lynxeye, 192 channels at 2.95°). Transmission electron microscopy (HRTEM) was performed with a JEOL JEM-ARM200F microscope fitted with a high-angle annular dark-field (HAADF) detector and an energy-dispersive spectrometer (EDS) for elemental analysis. The Brunauer-Emmett-Teller (BET) surface area was determined with N_2 as the adsorbate at 77.3 K using a Quantachrome Instruments v11.0 system (adsorption/desorption equilibration: 60 s). Fourier-transform infrared spectroscopy (FT-IR) was carried out with a Bruker Hong Kong Limited ALPHA model Fig. 1.

2.3. Preparation of alginate-chitosan beads (gCS-AG beads)

To prepare the alginate solution, dental-grade alginate powder was first ground into a fine powder and soaked in EDTA 0.01 M solution overnight. Then, 1.5 g of the alginate powder was dissolved in 25 mL of distilled water. Cold water was used to slow down the gelation process and ensure uniform dispersion before further processing. The calcium chloride-chitosan solution was prepared by dissolving 0.7 g of calcium chloride in 100 mL of distilled water. In a separate container, 1 g of chitosan was dissolved in 50 mL of 1 % acetic acid. The chitosan solution was then added to the calcium chloride solution, and the mixture was stirred continuously for 2 h to ensure homogeneity. The prepared alginate solution was drawn into a syringe fitted with an 18 G needle for bead formation. The syringe was positioned approximately 10 cm above the beaker containing the calcium chloride-chitosan solution, and the alginate solution was carefully dropped into the mixture at a consistent rate. This controlled addition facilitated the formation of uniform spherical beads. The beads were then stirred at 180 rpm for 2 h to allow complete crosslinking. Following this, they were filtered and washed thoroughly with sodium hydroxide solution to remove any residual unreacted components. The beads were further rinsed with distilled water until the pH of the wash solution reached neutral. For drying, the beads were initially air-dried at room temperature overnight. They were subsequently dried in an oven at 60 °C for 2 h to ensure complete moisture removal. The final dried beads were then stored in a desiccator until further use.

During the bead formation process, calcium chloride not only crosslinks alginate through ionic interactions with carboxyl groups but may also interact with the amino groups of chitosan, especially under acidic conditions where chitosan is positively charged. Calcium ions can further enhance the crosslinking between alginate and chitosan, thereby improving the mechanical stability and surface structure of the beads. Although this was not the study's primary focus, its potential impact on bead integrity and adsorption performance warrants further investigation.

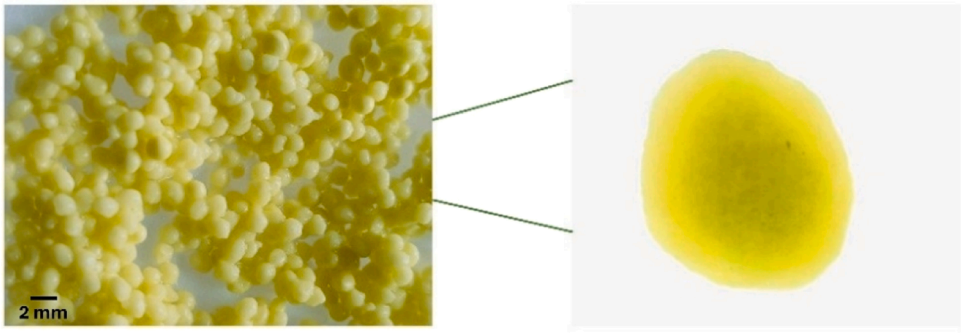

Fig. 1. Appearance of beads synthesized from irradiated chitosan and alginate (gCS-AG Beads) under Stereo Microscope.

2.4. Adsorption experiments

A 25 mL solution of CR (Congo Red) was prepared with a concentration of 100 mg/L. To this solution, 0.1 g of gCS-AG Beads, which act as adsorbents, were added. The mixture was stirred thoroughly to ensure even distribution of the beads throughout the solution. To assess the extent of adsorption, samples were taken from the solution after a specified contact time and filtered to remove the beads. The absorbance of the resulting filtered samples was then measured using *An sp*-UV200 UV/VIS Spectrophotometer set to a wavelength of 498 nm (slit width: 1 nm). This wavelength is optimal for detecting the presence of CR in the solution. To adjust the pH of the solutions for optimal adsorption conditions, a universal pH buffer capable of stabilizing the pH within the range of 2 to 12 was used (Souri et al., 2013; Martini et al., 2018; Kuras et al., 2017). This adjustment was crucial, as pH can significantly affect the adsorption characteristics of the adsorbents. Finally, the efficiency of adsorption was evaluated by applying a formula to calculate the percentage removal of congo red from the solution. This methodology allowed for a comprehensive examination of the adsorption process and helped in determining the effectiveness of the gCS-AG Beads in removing contaminants.

$$Removalefficiency = [(C_0 - -C) / C_0] \times 100$$

Where C_0 is the initial concentration of congo red, C is the solution concentration after adsorption at any time (Dinh et al., 2021; Yang et al., 2022; Wu et al., 2019). The Experimental section has been revised to provide more detailed descriptions of the procedures, including: pH Adjustment: A universal buffer was used to control the solution pH within the range of 2–12. The pH values were verified using a calibrated digital pH meter. Contact Time: Adsorption experiments were conducted at multiple contact times (e.g., 5, 15, 30, 60, 90, and 120 min) to analyze the kinetic behavior of the process. Adsorbent Dosage: Various amounts of gCS-AG beads (0.05 g, 0.1 g, and 0.2 g) were tested in 25 mL Congo Red solution (100 mg/L) to determine the optimal dosage. Adsorption Measurement: The remaining CR concentration was measured using a UV–Vis spectrophotometer at 498 nm. The adsorption efficiency was calculated based on the standard removal efficiency formula. Temperature Control: All experiments were conducted at ambient room temperature (25 ± 2 °C) to ensure consistency throughout the trials.

3. Results and discussion

3.1. Characterization of gCS-AG beads

The synthesis process of Alginate-Chitosan beads (gCS-AG beads) was thoroughly examined. Chitosan solutions were prepared using both non-irradiated and irradiated chitosan. The irradiated chitosan dissolved more easily and rapidly compared to the non-irradiated variety, indicating that the irradiation process enhanced the solubility of chitosan. After preparing the chitosan solution, alginate was introduced, and the mixture was added dropwise into a calcium chloride solution, which facilitated the formation of cross-linked beads. The resulting beads had an average size of approximately 2 mm, as confirmed through stereomicroscopic examination. The beads exhibited a layered structure, with the outermost layer made of irradiated chitosan. This strong and distinct chitosan coating on the alginate core was evident in the stereo microscope images, demonstrating the structural integrity and uniformity of the beads.

The HRTEM image displays a parallel arrangement on the surface, indicating a crystalline structure within the gCS-AG beads (Fig. 2). This orderly atomic arrangement confirms their crystalline properties at the nanoscale level. The visible D spacing (distance between crystal planes) allows for the calculation of crystal size, aiding in a deeper understanding of the chitosan-alginate bead structure. Furthermore, the image underscores the uniformity and completeness of the crystal arrangement, offering insights into the material's organized structure.

The analysis of gCS-AG beads (Alginate-Chitosan Beads) using Backscattered Electron Imaging (BEI) and High-Angular Annular Dark Field Scanning Transmission Electron Microscopy (HAADF-STEM) reveals significant structural insights, particularly the presence of surface pores. This porosity enhances the material's surface area and improves its adsorption properties, allowing for more effective capture of pollutants and contaminants. The rough surface observed in BEI and the high atomic contrast seen in HAADF-STEM indicate that the gCS-AG Beads have a complex and well-organized porous structure. These features make them suitable for applications like wastewater treatment, where efficient contaminant removal is essential. Overall, the findings emphasize the potential of gCS-AG beads for pollution control and environmental cleanup through their ability to adsorb harmful substances.

The SAED (Selected Area Electron Diffraction) image shows spots arranged in a ring or star-like pattern, indicating the crystallographic structure of the sample. Bright spots suggest a well-ordered crystalline structure, allowing for analysis of D spacing, or the distance between crystal planes. This ring-like arrangement helps determine if the material is a single crystal or polycrystalline. The D spacing value of 51/nm corresponds to a spacing of about 5 Å, indicating the periodicity of the crystal planes. This information is crucial for assessing the material's crystallinity and is useful for applications in adsorption and materials engineering. The EDS analysis (Table 1) of gCS-AG beads revealed the presence of elements such as carbon (C), nitrogen (N), oxygen (O), and calcium (Ca). These elements indicate the composition of chitosan and alginate within the structure. Their presence confirms that the beads have a well-organized structure, demonstrating that gCS-AG beads can be effectively synthesized by binding irradiated chitosan with alginate to form the bead structure.

The EDS analysis of gCS-AG beads prior to usage reveals the presence of key elements, including Carbon (C), Nitrogen (N), Oxygen (O), and Calcium (Ca). The carbon content in the gCS-AG beads is approximately 0.16 %, which aligns with the presence of chitosan, a biopolymer that contains amine groups (-NH_2). The nitrogen content is measured at 0.33 %, indicating its role in the adsorption process and interactions with

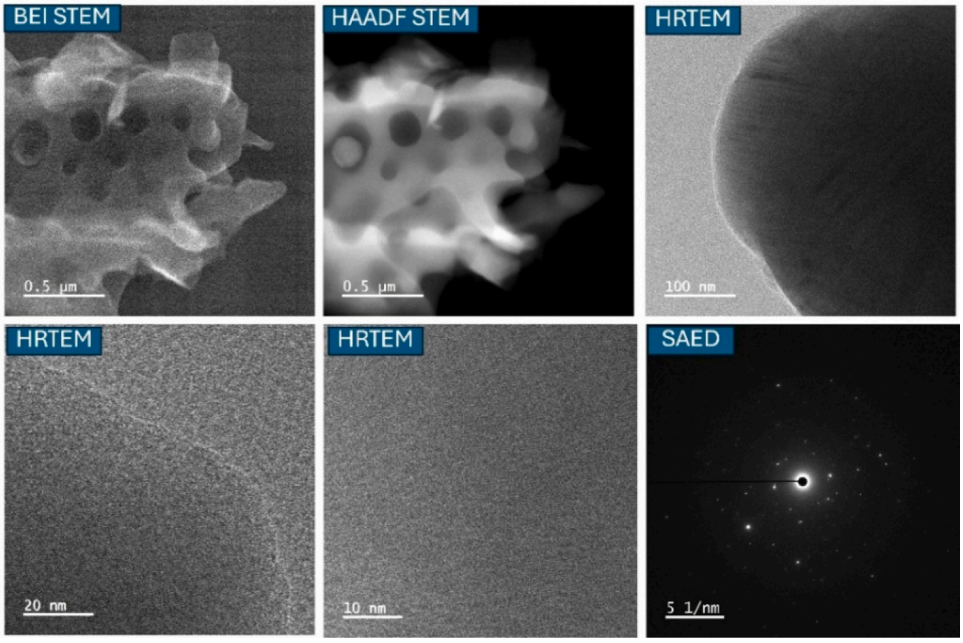

Fig. 2. BEI-STEM, HAADF-STEM, HRTEM, and SAED images of gCS-AG beads.

Table 1
EDS analysis of the catalysts.

Catalysts	Atomic%					
	C	N	O	Ca	S	Na
AG- beads	0.08	–	0.33	0.07	–	–
CS-AG beads	0.07	0.01	0.25	0.04	–	–
gCS-AG beads	0.16	0.04	0.33	0.06	–	–
After used gCS-AG beads	0.11	0.03	0.25	0.08	0.01	0.03

other components in the bead structure. The oxygen content is also 0.33 %, which is associated with the hydroxyl (-OH) groups found in both chitosan and alginate. Furthermore, the calcium content is 0.04 %, suggesting that calcium from alginate contributes to bond formation with carboxyl groups (COO^-), thereby enhancing the overall structure of the beads. In the EDS mapping (Fig. 3), the distribution of elements such as Carbon (C), Nitrogen (N), Oxygen (O), and Calcium (Ca) provides a clearer understanding of the chemical composition of the beads. The abundant presence of Carbon indicates the incorporation of chitosan, which serves as the main component of the beads. Nitrogen is also prominently visible, confirming the presence of amino groups ($-NH_2$) that play a vital role in the adsorption process, especially for charged contaminants. The distribution of Oxygen, associated with the presence of hydroxyl groups (-OH), demonstrates that these groups enhance the bead's ability to interact with pollutants. Furthermore, Calcium, an integral part of the calcium alginate structure, is present and contributes to the beads' structural integrity while enhancing interactions with carboxyl groups (COO^-). This combination makes the material more stable and effective for adsorption.

The BET analysis and the pore volume versus pore diameter graph (Table 2) clearly illustrate the differences in the porosity and surface area of gCS-AG beads, CS-AG beads, and AG beads. Among them, gCS-AG beads (red) demonstrate the highest pore volume and surface area, measuring 68.045 m^2/g, which significantly surpasses that of CS-AG beads (55.275 m^2/g) and AG beads (51.447 m^2/g). This increased surface area enhances the adsorption capacity of gCS-AG beads, confirming their effectiveness in adsorbing pollutants. Additionally, the pore volume of gCS-AG beads is 0.083 cm^3/g, the highest among the three types, which further supports their superior adsorption efficiency. The average pore diameter of gCS-AG beads is 2.971 nm, slightly larger than that of the CS-AG and AG beads, confirming optimal porosity for contaminant adsorption. In conclusion, gCS-AG beads exhibit superior surface area, pore volume, and porosity, making them the most effective material for pollutant adsorption and wastewater treatment applications.

The nitrogen adsorption-desorption isotherm results (Fig. 4A) for AG beads, CS-AG beads, and gCS-AG beads indicate that gCS-AG beads have the highest surface area and the most effective adsorption characteristics among all the materials tested. This type of isotherm exhibits a hysteresis loop between the adsorption and desorption graphs, indicating the presence of pore filling or nitrogen trapping in voids that are not easily emptied. This finding aligns with the Type IV isotherm, which suggests a mesoporous structure with medium-sized pores that are efficient at adsorbing nitrogen at higher relative pressures.

The X-ray diffraction (XRD) analysis of five samples gCS-AG beads, CS-AG beads, AG beads, gCS (irradiated chitosan), and CS (non-irradiated chitosan) reveal significant differences in crystallinity (Fig. 4B). gCS-AG beads show distinct peaks at 20.2° and 36.4°, indicating a high degree of crystallinity. In comparison, gCS displays clearer peaks at 10.6° and 20.1°, suggesting that irradiation improves chitosan's crystallization, while CS has diffused peaks that denote poorer crystallinity. γ-Irradiation reduces fibrillar curvatures in chitosan, leading to a more compact crystalline arrangement (Pati et al., 2021; Kang et al., 2007). Overall, gCS-AG beads exhibit the most ordered structure, in contrast to the less defined CS-AG beads and the amorphous AG beads.

The FTIR spectra (Fig. 4C) of gCS-AG beads, CS-AG beads, and AG beads show carboxyl groups (COO^-) at 1410 cm^{-1} and O—H and C—O bands at 3329 cm^{-1} and 1599 cm^{-1}, confirming the presence of hydroxyl and carboxyl groups in gCS-AG beads. The peak at 1410 cm^{-1} corresponds to the asymmetric stretching of COO^- groups in alginate, which may participate in electrostatic interactions with protonated amine groups of chitosan. This analysis suggests that γ-irradiation induces chemical modifications in chitosan and alginate materials, resulting in increased functional groups. The gCS-AG beads, made from irradiated chitosan (gCS) and alginate (AG), exhibit more pronounced carboxyl groups at 1411 cm^{-1} compared to the less affected CS-AG beads, which consist of non-irradiated chitosan (CS). These findings align with prior research indicating that γ-irradiation cleaves glycosidic bonds, forming hydroxyl and carboxyl groups. The increased presence of these functional groups in gCS-AG beads enhances their adsorption capacity for

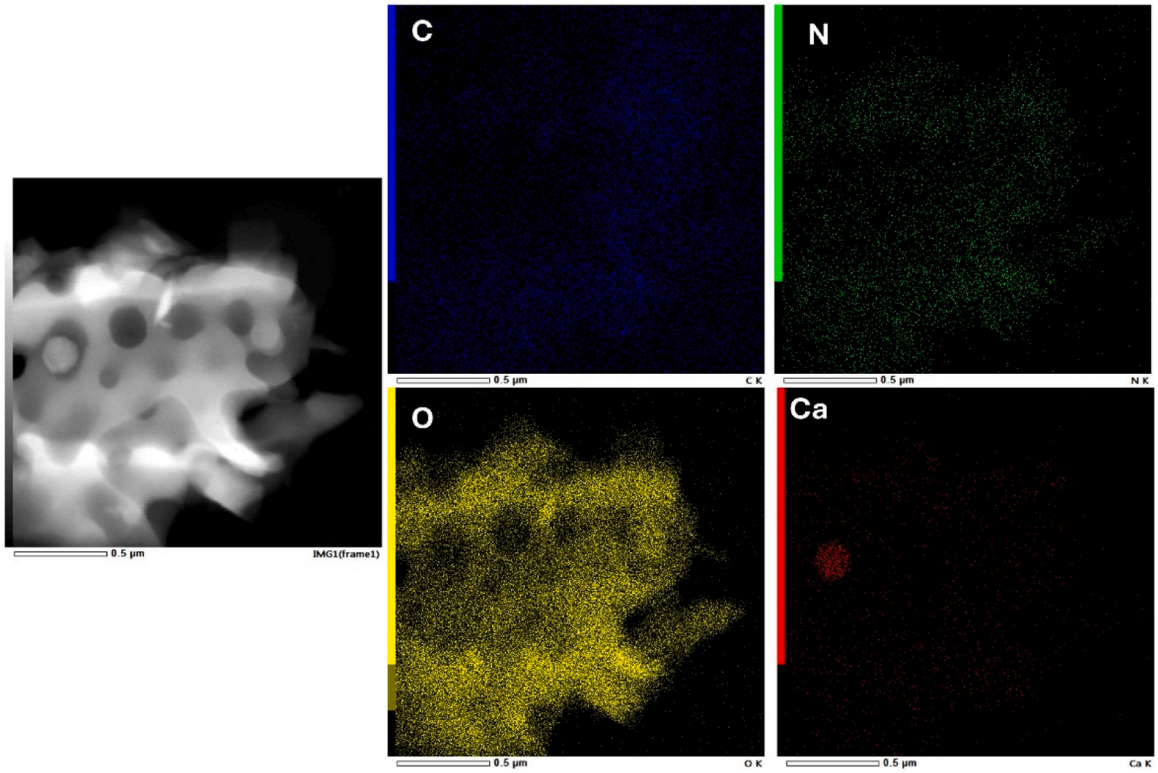

Fig. 3. HAADF-STEM and EDS mapping of gCS-AG beads.

Table 2
Textural properties of the catalysts (BET and BJH methods). Notes: aBET surface area,bBJH methods.

Samples	Surface Area[a], S_{BET} (m^2/g)	Pore Volume[b], Vp (cm^3/g)	Average Pore diameter[b], Dp (nm)
AG- beads	51.447	0.058	2.969
CS-AG beads	55.275	0.070	2.970
gCS-AG beads	68.045	0.083	2.971

contaminants, confirming improved performance due to the structural changes induced by γ-irradiation (Kang et al., 2007). In the XRD analysis of the gCS-AG beads, the characteristic diffraction peaks of chitosan were not clearly observable. This can be attributed to two main factors. First, the gamma-irradiated chitosan was applied as a thin outer coating on the alginate beads, resulting in a lower overall mass fraction compared to the bulk alginate. Second, the highly crystalline signals from alginate may have overlapped with or masked the weaker signals from the irradiated chitosan. Moreover, gamma irradiation can reduce the crystallinity of chitosan due to chain scission, which contributes to the diminished XRD peaks. Despite the weak or absent peaks in the XRD pattern, the presence of chitosan in the gCS-AG beads is clearly supported by other characterization methods. FTIR analysis revealed distinct absorption bands associated with amino and carboxyl groups, which are characteristic of gamma-irradiated chitosan. Additionally, EDS analysis confirmed the presence of nitrogen (N) atoms in the composite beads, which is a unique elemental marker for chitosan and is absent in pure alginate. These results collectively validate the successful incorporation of gamma-irradiated chitosan into the biopolymer bead matrix.

3.2. Adsorption

The experimental results in Fig. 5A show that gCS-AG beads achieve maximum adsorption of Congo Red (CR) at pH 2. At this pH, the beads not only adsorb congo red effectively but also promote its structural degradation. This interaction is likely due to the carboxyl and hydroxyl groups formed during γ-irradiation, which react with congo red in the acidic environment. As pH increases to 6 or 7, the adsorption efficiency declines because the functional groups become less effective, and degradation occurs less efficiently. Thus, pH 2 is optimal for both the adsorption and degradation of congo red, highlighting the advantageous chemical interaction under acidic conditions. The high adsorption efficiency at pH 2 is due to the protonation of amine groups ($–NH_3^+$) in chitosan, enhancing electrostatic attraction with the negatively charged sulfonate groups in congo red. The increased adsorption at lower pH is typically attributed to the protonation of functional groups on the adsorbent surface, which can lead to stronger interactions with the anionic congo red dye. For instance, research by Hua et al. (2023) demonstrated that at pH 2–3, the adsorption capacity of orange peel biochar modified with CTAB for Congo Red dye increased significantly compared to neutral or basic conditions (Hua et al., 2023). Similarly, Ige et al. (2024) found that acidic conditions favored the adsorption process due to enhanced electrostatic interactions between the adsorbent and the dye molecules (Ige et al., 2024; Imessaoudene et al., 2023). The gCS-AG beads exhibited optimal congo red dye removal efficiency at pH 2. This consistency with existing literature supports the effectiveness of acidic conditions in enhancing the adsorption of congo red dye.

From Fig. 5B, The graph comparing the adsorption of Congo Red (CR) by various materials non-irradiated chitosan (CS), γ-irradiated chitosan (gCS), alginate (AG) beads, CS-AG beads, and gCS-AG beads shows that gCS-AG beads achieve the highest adsorption efficiency, removing over 80 % of CR. This exceptional capacity is due to the γ-irradiation process, which enhances chitosan's structure and increases functional groups like carboxyl and hydroxyl, improving its ability to absorb pollutants. In contrast, CS-AG beads, made from non-irradiated

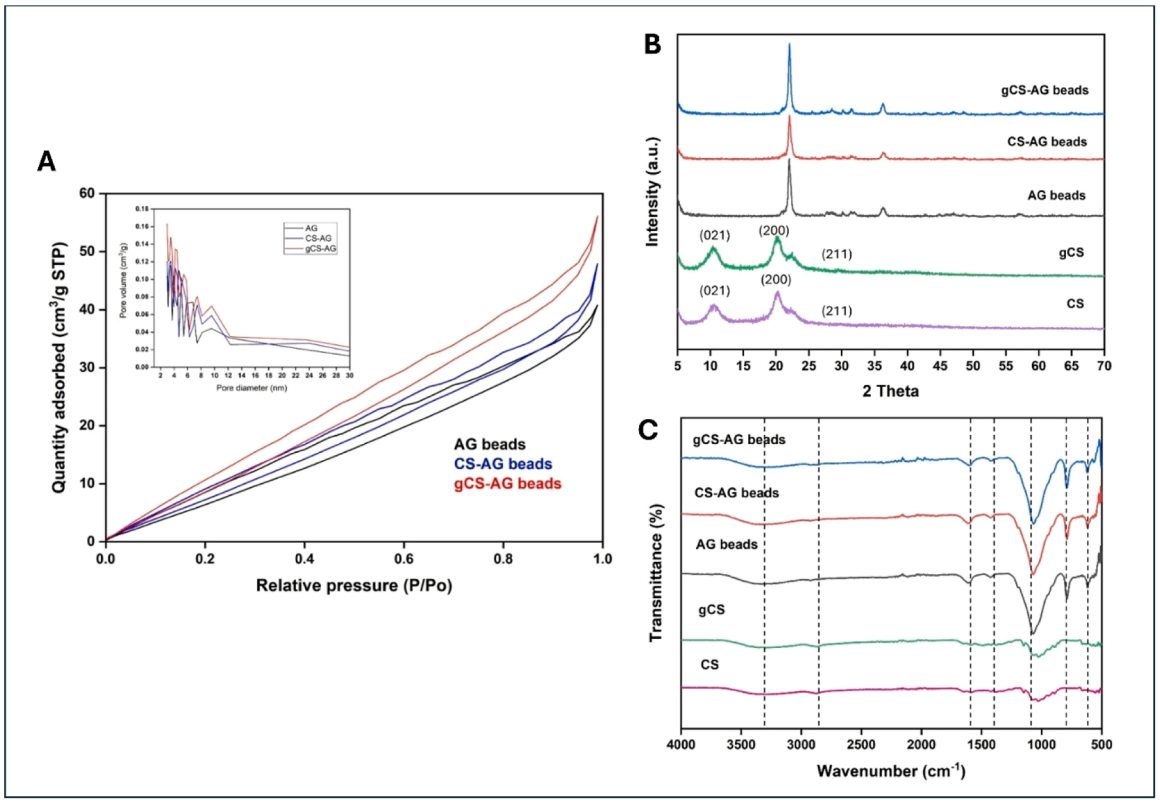

Fig. 4. A. The nitrogen adsorption–desorption isotherms of AG- beads, CS-AG beads and gCS-AG beads. B. The XRD patterns of AG- beads, CS-AG beads, gCS-AG beads, gCS, and CS. C. FTIR spectra of AG- beads, CS-AG beads, gCS-AG beads, gCS, and CS.

chitosan and alginate, demonstrate moderate adsorption capacity due to the lack of structural enhancements. AG beads, CS, and gCS show the lowest efficiencies, but gCS outperforms CS.

The results in Fig. 5C illustrate the impact of adsorbent dosage on the removal of Congo Red (CR). At a dosage of 0.1 g of gCS-AG beads, the removal percentage reaches about 80 %, indicating effective adsorption. However, increasing the dosage further does not significantly improve removal rates, suggesting that 0.1 g is optimal. Therefore, we will use 0.1 g of adsorbent in future experiments for the best performance and material usage balance. The experimental results shown in Fig. 5D of the reuse of the gCS-AG beads catalyst show that gCS-AG beads can be reused up to 10 cycles while maintaining a Congo Red removal efficiency of over 70 %. This indicates the durability and consistent performance of the gCS-AG beads in adsorbing Congo Red, even after multiple uses. The gCS-AG beads demonstrate an effective dye absorption process, as evidenced by their color change from light green before adsorption to orange after adsorption. Even after multiple reuse cycles, the beads retain their orange color, indicating their continued effectiveness in adsorbing Congo Red. The step-like pattern in Fig. 5C, where adsorption efficiency does not increase smoothly with adsorbent dosage, can be attributed to two main factors:

(1) Bead Agglomeration: At higher dosages, gCS-AG beads tend to clump together, reducing the effective surface area available for adsorption. This phenomenon has been observed in similar systems, such as activated carbon, where an increase in adsorbent mass results in a decrease in adsorption per unit mass (Wekoye et al., 2020). (2) Saturation of Active Sites: Increasing the adsorbent dosage while keeping the dye concentration constant can leave many active sites unused, resulting in a plateau in removal efficiency. Subhan et al. (2022) noted that excessive adsorbent beyond the optimal dosage does not significantly enhance dye removal (Subhan et al., 2022). Therefore, the step-like increase in adsorption efficiency reflects the physical and chemical limitations of the system and will be clarified in the revised discussion section.

The analysis of gCS-AG beads using BEI-STEM, HRTEM, and SAED reveals that the beads maintain their structure and performance even after multiple adsorption cycles (Fig. 6). While the BEI-STEM images show changes in surface texture due to contaminant interactions, these alterations do not affect the overall integrity of the beads. The reusability procedure, including desorption with 0.1 M NaOH, rinsing, and pH adjustment. HRTEM images indicate that the atomic arrangement remains well-organized, confirming the retention of the crystalline structure crucial for effective adsorption. Additionally, SAED patterns show consistent diffraction points, indicating that the crystalline structure is intact. Overall, the results confirm that gCS-AG beads can be reused multiple times without significant degradation, highlighting their durability and long-term effectiveness in adsorption applications. After utilizing the gCS-AG Beads for the adsorption of Congo Red, the EDS analysis (Table 1) reveals significant changes in the elemental composition. The carbon content decreases from 0.16 % to 0.11 %, which suggests that some carbon components may have participated in the adsorption process by interacting with the Congo Red dye or other contaminants. The nitrogen content also decreases from 0.33 % to 0.25 %, possibly indicating that nitrogen plays a role in the interaction between chitosan and the dye. Similarly, the oxygen content declines from 0.33 % to 0.25 %, implying alterations in the hydroxyl (-OH) groups during the adsorption process. Additionally, the calcium (Ca) content increases from 0.04 % to 0.08 %, highlighting stronger interactions between calcium derived from alginate and carboxyl groups (COO^-) during adsorption. Furthermore, sulfur (S) is detected at 0.01 % and sodium (Na) at 0.03 %, which may indicate interactions between sulfonate (SO_3^-) groups from the Congo Red dye and the adsorption material. The EDS analysis of gCS-AG beads before and after use shows notable changes in elemental composition. The increase in calcium indicates stronger interactions with carboxyl groups, while the decrease in nitrogen and carbon suggests structural changes during adsorption.

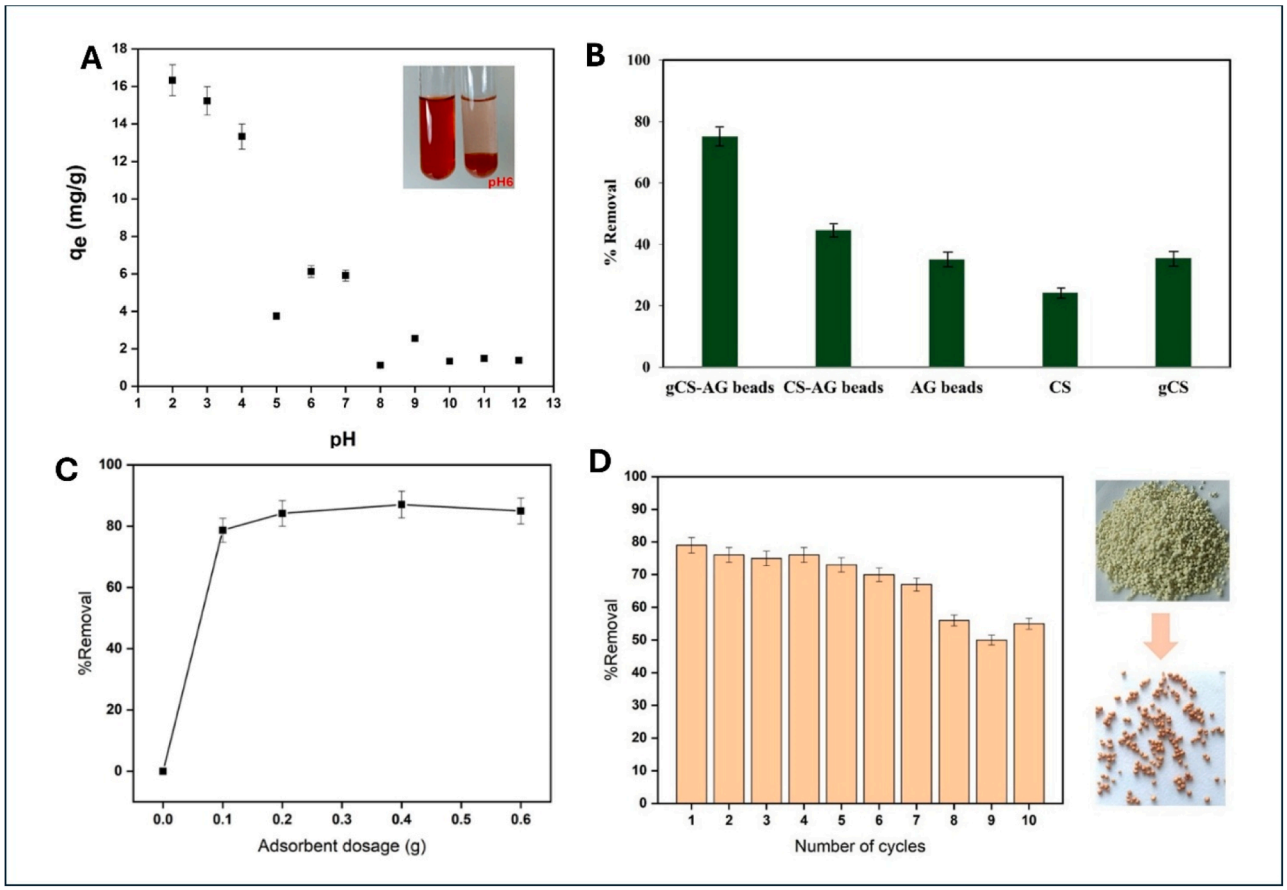

Fig. 5. A. Effect of solution pH value on the adsorption of congo red, (gCS-AG beads 0.1 g, [CR] 100 mg/L, Time 60 min). B. Comparison of the adsorption of congo red by CS, gCS, AG beads, CS-AG beads, and gCS-AG beads, (Biopolymer beads 0.1 g, [CR] 100 mg/L, Time 60 min). C. Effect of adsorbent dosage on adsorption of congo red ([CR] 100 mg/L, pH 2, Time 60 min). D. Reuse of gCS-AG beads catalyst.

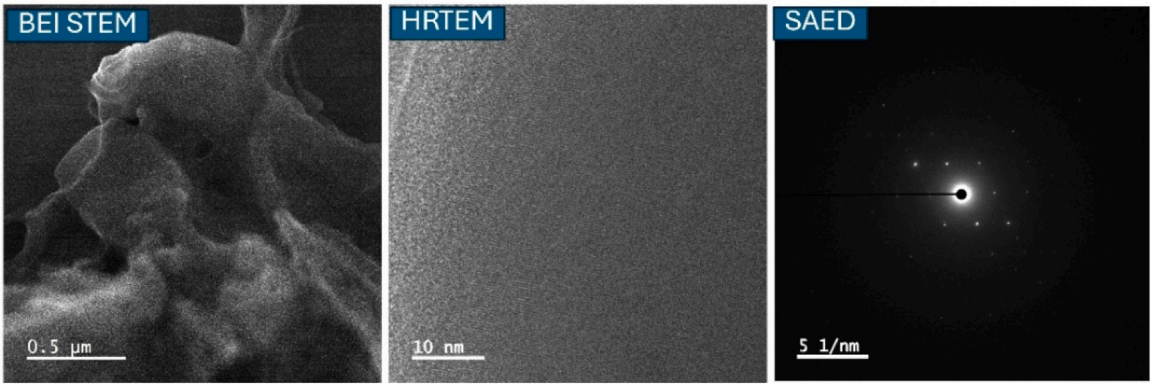

Fig. 6. Images from BEI-STEM, HRTEM, and SAED taken after used gCS-AG beads.

Additionally, the presence of sulfur and sodium highlights the interactions between the dye and the adsorbent. Overall, these changes enhance the gCS-AG beads' effectiveness in removing contaminants during the adsorption of Congo Red.

The schematic illustrates (Fig. 7) the dual-function behavior of gCS–AG beads in the removal of Congo Red (CR) from aqueous solution. The adsorption mechanism involves electrostatic attraction between the protonated amino groups ($–NH_3^+$) on chitosan and the sulfonate groups ($–SO_3^-$) of CR, as well as hydrogen bonding interactions with hydroxyl and amine groups on the biopolymers. Additionally, physical entrapment of dye molecules within the porous bead structure contributes to the uptake. The degradation mechanism is facilitated by reactive radicals (e.g., •OH, $•O_2^-$) formed during gamma irradiation, which attack the azo bond ($–N=N–$) of CR, leading to partial breakdown of the dye structure, especially under acidic conditions. These synergistic interactions account for the enhanced dye removal efficiency of the gCS–AG composite beads (Rabeie et al., 2025).

3.2.1. *Adsorption isotherms*

This study used the Extended Langmuir Isotherm equation for data fitting that created a graph plotting the adsorption quantity (Qe) against the remaining concentration (Ce) of congo red dye, demonstrating excellent adsorption behavior. The Extended Langmuir Isotherm equation describes adsorption behavior involving competition between

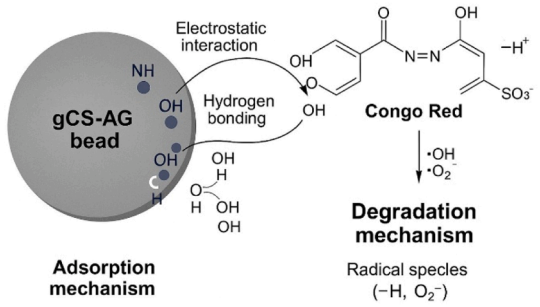

Fig. 7. Proposed adsorption and degradation mechanisms of Congo Red on gamma-irradiated chitosan–alginate (gCS–AG) bio-beads.

multiple sites or adsorption mechanisms. The equation is as follows:

$$Qe = \frac{Q_{max} K_L C_e}{1 + K_L C_e}$$

Where Qe = Amount of adsorbate (mg/g) adsorbed onto the surface at equilibrium concentration Ce, Ce = Concentration of the adsorbate remaining in the solution (mg/L) after adsorption, Q_{max} = Maximum adsorption capacity (mg/g) that the adsorbent can achieve at the highest concentration, and K_L = The Langmuir binding constant.

Applying the Extended Langmuir Isotherm equation (Subhan et al., 2022; Pathania et al., 2017) yielded an R^2 value of 0.97317 and a χ^2 value of 0.8688. These results suggest that the adsorption of congo red is well described by this model, indicating that the beads exhibit a heterogeneous surface with competitive adsorption sites (Putro et al., 2017) (Fig. 8A). Adsorption isotherms, the maximum adsorption capacity q_{max} = 18.50 $mg.g^{-1}$. Langmuir isotherm was the isotherm model closest to the experimental values for the maximum adsorption capacity. The compatibility of the Extended Langmuir Isotherm equation suggests that the adsorption of congo red dye onto alginate-chitosan beads does not adhere to the classical Langmuir model. This is likely due to several competing adsorption mechanisms that target the same binding sites. One key mechanism is electrostatic attraction, where the positive charges on chitosan interact with the negative charges of congo red, facilitating the dye's attachment to the bead surface. Also, hydrogen bonding occurs between the functional groups of chitosan and alginate, strengthening the bond between the dye and the beads. Ion exchange also contributes to the overall adsorption process, as ions are exchanged between the adsorbent and the dye. Furthermore, π-π stacking interactions between the azo groups of congo red and the adsorbent's structure enhance the dye's effective binding. These findings demonstrate that the alginate-chitosan beads possess a complex structure, allowing them to efficiently adsorb contaminants through multiple mechanisms, thereby improving their ability to remove pollutants.

While the initial analysis employed the Extended Langmuir isotherm, which is suitable for mixed adsorption behaviors across homogeneous and heterogeneous surfaces, additional isotherm models were applied to enhance the mechanistic interpretation of the adsorption process. The Freundlich isotherm (Fig. 8B) is an empirical model appropriate for adsorption on heterogeneous surfaces and multilayer coverage, expressed as: $\log Q = \log K_F + 1/n \log Ce$. The Temkin isotherm (Fig. 8C) accounts for the decreasing adsorption of energy with increasing surface coverage and is represented as: $Qe = B \ln A + B \ln Ce$. The high R^2 values for both models (Freundlich: 0.958, Temkin: 0.969) suggest that congo red adsorption onto gCS-AG beads involves heterogeneous site interactions and a non-constant heat of adsorption, which complements the Extended Langmuir interpretation and supports a more comprehensive understanding of the system.

3.2.2. *Adsorption kinetics*

Adsorption kinetics of congo red on gCS-AG beads was examined using pseudo-second-order model which gives a linear form as follows:

$$\frac{t}{q_t} = \frac{1}{kq_e^2} + \frac{t}{q_e}$$

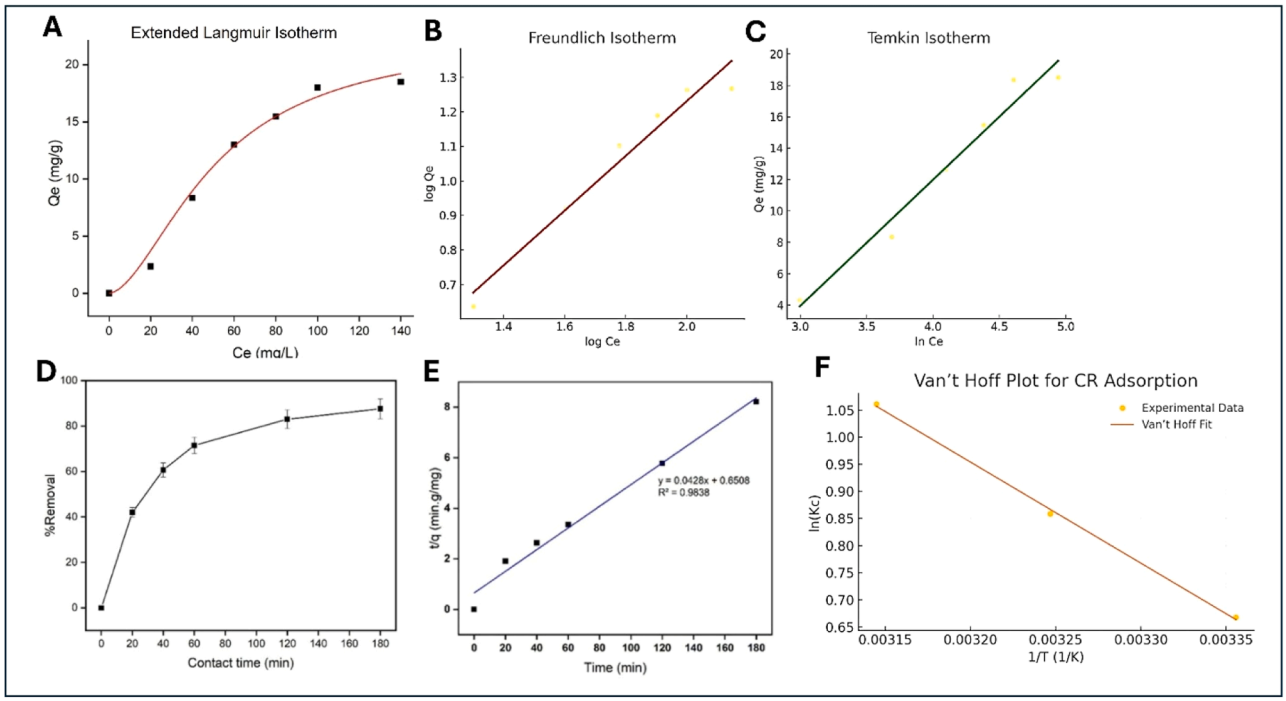

Fig. 8. A. Adsorption isotherms of CR on gCS-AG beads (adsorbent dosage 0.1 g, [CR] 0 −140 mg/L, Time 60 min, pH 2). B. Freundlich isotherm. C. Temkin isotherm linear plots for Congo Red adsorption. D. Effect of contact time on the adsorption of congo red. E. The pseudo-second-order adsorption kinetic equation (gCS-AG beads 0.1 g, [CR] 100 mg/L, pH 2). F. Van't Hoff plot of ln(Kc) versus 1/T for the adsorption of Congo Red onto gCS-AG beads. (Kc = equilibrium constant, R = 8.314 J/mol·K, T = temperature in Kelvin).

where k (g^{-1} min^{-1}) is the rate constant of pseudo-second-order adsorption; q_e and q_t (g/mg) are the amounts of congo red adsorbed at equilibrium and time t (min), respectively (Wekoye et al., 2020; Revellame et al., 2020; Jabar et al., 2020).

Fig. 8E shows the formula for calculating the adsorption kinetics of Congo Red using the pseudo-second-order model, which helps estimate kinetic parameters. In Fig. 8D, the first graph illustrates the percentage removal of Congo Red as contact time increases. There is a rapid rise in removal efficiency initially, suggesting that a large amount of Congo Red is adsorbed quickly. However, as time progresses, this rate slows and reaches a plateau, indicating that adsorption sites are becoming occupied. The second graph in Fig. 8E represents the pseudo-second-order kinetic model, demonstrating a linear relationship between adsorption capacity (t/q) and time (t). The straight line and high linear correlation ($R^2 = 0.9838$) confirm that the adsorption process follows this model, where the rate is proportional to the square of the number of occupied sites. Overall, these findings indicate that the adsorption of Congo Red onto gCS-AG beads follows a pseudo-second-order kinetic model, with efficiency increasing over time until equilibrium is reached. The results emphasize that the availability of adsorption sites on the beads primarily controls the process.

The slope and intercept were used to calculate the enthalpy (ΔH°) and entropy (ΔS°) changes, confirming the endothermic and spontaneous nature of the process (Fig. 8F). To understand the nature of CR adsorption onto gCS-AG beads, thermodynamic parameters (ΔH°, ΔS°, and ΔG°) were calculated using the Van't Hoff equation (Foo & Hameed, 2010). The thermodynamic parameters for CR adsorption onto gCS-AG beads were evaluated using the Van't Hoff equation. The positive enthalpy change ($\Delta H^\circ = +13.27$ kJ/mol) indicates an endothermic process, suggesting enhanced adsorption at elevated temperatures. The positive entropy ($\Delta S^\circ = +53.88$ J/mol·K) implies increased randomness at the solid–liquid interface during adsorption. Moreover, the negative Gibbs free energy values at all tested temperatures (ΔG° ranging from –2.73 to –3.81 kJ/mol) confirm that the adsorption process is spontaneous and thermodynamically favorable.

Comparative maximum adsorption capacities (q_{max}) of bead-form adsorbents for Congo Red removal. Although our material has a lower maximum adsorption capacity (18.5 mg/g), its advantages in terms of sustainability, biodegradability, and practical usability highlight its potential applications. Several studies utilizing bead-form adsorbents for Congo Red removal report higher q_{max} values, such as cellulose/chitosan hydrogel beads (~40 mg/g) and CS-DE@CA composite beads (48.4 mg/g) (Zhao & Shen, 2023). Although these outperform our gCS-AG beads (18.5 mg/g), our adsorbents offer distinct advantages in biodegradation, dental waste valorization, ease of bead separation, and overall sustainability, making them suitable alternatives in real-world applications.

4. Conclusion

This study investigated the adsorption properties of Congo Red dye using γ-irradiated chitosan (gCS) and alginate (AG) beads, referred to as gCS-AG beads, in comparison to natural chitosan (CS) and AG beads, labeled as AG beads. A variety of analytical techniques were employed, including FTIR, XRD, BET, and TEM (which includes HRTEM, SAED, and BEI STEM), to evaluate the properties and effectiveness of these beads in adsorbing Congo Red dye. The results demonstrated that gCS-AG beads exhibited the highest adsorption efficiency, achieving a removal percentage of up to 80 % at a pH of 2. Furthermore, these beads showed excellent reusability, maintaining high adsorption efficiency even after 10 cycles of use, without significant degradation of their structure. TEM analysis, through BEI STEM, HRTEM, and SAED, confirmed that the beads sustained their well-organized structure after being used. FTIR analysis indicated the formation of carboxyl (COO^-) and hydroxyl (OH) groups during the γ-irradiation process, which enhanced the material's adsorption capability. The study of adsorption kinetics revealed that the process followed a pseudo-second-order model, with adsorption capacity rapidly increasing in the initial stages and then leveling off once the adsorption sites were saturated. Overall, these findings confirm that gCS-AG beads have a highly suitable structure for adsorbing pollutants, with γ-irradiation treatment significantly improving their adsorption capacity and stability for repeated use. While the gCS-AG beads showed promising adsorption and partial degradation capabilities, certain limitations should be addressed. The adsorption capacity ($q_{max} = 18.50$ mg/g) is lower than that of commercial activated carbon, and the optimal performance was observed only under acidic conditions (pH ~2), which may limit real-world applicability in neutral wastewater. Mechanical stability after long-term reuse should also be further examined. Nevertheless, the results indicate high potential for scale-up applications. The fabrication process is simple, cost-effective, and environmentally friendly, utilizing dental waste. Future work could explore performance in complex wastewater matrices, functional modification to enhance performance in neutral pH, and integration into continuous flow systems for real wastewater treatment.

CRediT authorship contribution statement

Prach Ponlawat: Writing – review & editing, Validation, Methodology, Investigation, Data curation. **Narawadee Prathum:** Visualization, Validation, Investigation, Formal analysis, Data curation. **Pitchapa Pittayavinai:** Visualization, Validation, Software, Resources, Investigation, Formal analysis. **Ranida Tuanudom:** Visualization, Validation, Software, Methodology, Investigation, Formal analysis. **Narudom Srisawang:** Visualization, Validation, Software, Project administration, Investigation. **Thongnard Kumchai:** Writing – review & editing, Validation, Project administration, Methodology, Formal analysis, Conceptualization. **Phitchan Sricharoen:** Visualization, Validation, Resources, Methodology, Investigation, Formal analysis. **Ekasith Somsook:** Visualization, Validation, Supervision, Investigation, Funding acquisition, Conceptualization. **Titiya Meechai:** Writing – review & editing, Writing – original draft, Supervision, Methodology, Investigation, Formal analysis, Conceptualization.

Declaration of competing interest

The authors declare that they have no known competing financial interests or personal relationships that could have appeared to influence the work reported in this paper.

Acknowledgements

Bangkokthonburi University and NANOCAST Laboratory, Center for Catalysis Science and Technology (CAST) supported this study.

Funding Statement

No Funding.

Data availability

The data that has been used is confidential.

References

Abourehab, M. A. S., et al. (2022). Alginate as a Promising Biopolymer in Drug Delivery and Wound Healing: A Review of the State-of-the-Art. *International journal of molecular sciences, 23*.

Alavinia, S., Ghorbani-Vaghei, R., Asadabadi, S., & Atrian, A. (2023). Sodium alginate/diethyleneamine-triazine-sulfonamide nanocomposite for adsorptive removal of Pb (II) and methyl violet from aqueous solutions. *Materials Chemistry and Physics, 293*, Article 126915.

Areerob, Y., et al. (2022). Novel gamma-irradiated chitosan-doped reduced graphene-CuInS2 composites as counter electrodes for dye-sensitized solar cells. *RSC Advances, 12*, 15427–15434.

Bhattacharyya, K. G., & Sharma, A. (2005). Kinetics and thermodynamics of Methylene Blue adsorption on Neem (Azadirachta indica) leaf powder. *Dyes and Pigments, 65*, 51–59.
Coura, J. C., Profeti, D., & Profeti, L. P. R. (2020). Eco-friendly chitosan/quartzite composite as adsorbent for dye removal. *Materials Chemistry and Physics, 256*, Article 123711.
Dinh, N. T., Vo, L. N. H., Tran, N. T. T., Phan, T. D., & Nguyen, D. B. (2021). Enhancing the removal efficiency of methylene blue in water by fly ash via a modified adsorbent with alkaline thermal hydrolysis treatment. *RSC Advances, 11*, 20292–20302.
Fathy, M., Selim, H., & Shahawy, A. E. L. (2020). Chitosan/MCM-48 nanocomposite as a potential adsorbent for removing phenol from aqueous solution. *RSC Advances, 10*, 23417–23430.
Foo, K. Y., & Hameed, B. H. (2010). Insights into the modeling of adsorption isotherm systems. *Chemical Engineering Journal, 156*, 2–10.
Haririan, Y., & Asefnejad, A. (2024). Biopolymer hydrogels and synergistic blends for tailored wound healing. *International Journal of Biological Macromolecules, 279*, Article 135519.
Hua, Z., Pan, Y., & Hong, Q. (2023). Adsorption of Congo red dye in water by orange peel biochar modified with CTAB. *RSC Advances, 13*, 12502–12508.
Ige, A. O., Ogunsile, B. O., Ore, O. T., & Olawade, D. B. (2024). Adsorption of congo red from aqueous solution using rice husk, calcined kaolin clay, and microwaved rice husk clay hybrid. *Discover Chemistry, 1*, 9.
Imessaoudene, A., et al. (2023). Adsorption Performance of Zeolite for the Removal of Congo Red Dye: Factorial Design Experiments, Kinetic, and Equilibrium Studies. *Separations*. https://doi.org/10.3390/separations10010057
Jabar, J. M., Odusote, Y. A., Alabi, K. A., & Ahmed, I. B. (2020). Kinetics and mechanisms of congo-red dye removal from aqueous solution using activated Moringa oleifera seed coat as adsorbent. *Applied Water Science, 10*, 136.
Kang, B., Dai, Y.-d., Zhang, H.-q., & Chen, D. (2007). Synergetic degradation of chitosan with gamma radiation and hydrogen peroxide. *Polymer Degradation and Stability, 92*, 359–362.
Karthikeyan, T., Rajgopal, S., & Miranda, L. R. (2005). Chromium(VI) adsorption from aqueous solution by Hevea Brasilinesis sawdust activated carbon. *Journal of Hazardous Materials, 124*, 192–199.
Keanjun, N., et al. (2024). Ultrasound-assisted formation of composite materials from fish scale waste hydroxyapatite in the presence of gamma-irradiated chitosan for the removal of malachite green. *RSC Advances, 14*, 29737–29747.
Koosha, S., Ghorbani-Vaghei, R., & Alavinia, S. (2025). Recyclable nano-CuI immobilized on UiO-66-NH2 coated with porous sodium alginate-polysulfonamide for synthesis of phenols. *Carbohydrate Polymer Technologies and Applications, 9*, Article 100665.
Kuras, M. J., Perz, K., & Kołodziejski, W. L. (2017). Synthesis, characterization and application of a novel zinc(II) ion-imprinted polymer. *Polymer Bulletin, 74*, 5029–5048.
Mahmoodi, N. M., Ghadirli, M. M., Hayati, B., Mahmoodi, B., & Rabeie, B. (2025). Synthesis of ZIF-8 composite (g-C3N4@ZIF-8/Ag3PO4) as a catalyst for the malachite green and tetracycline degradation. *Inorganic Chemistry Communications, 177*, Article 114345.
Martini, B. K., Daniel, T. G., Corazza, M. Z., & de Carvalho, A. E. (2018). Methyl orange and tartrazine yellow adsorption on activated carbon prepared from boiler residue: Kinetics, isotherms, thermodynamics studies and material characterization. *Journal of Environmental Chemical Engineering, 6*, 6669–6679.
Meechai, T., et al. (2023). *One-pot synthesis of iron oxide-Gamma irradiated chitosan modified SBA-15 mesoporous silica for effective methylene blue dye removal, 9*, Article e16178.
Pathania, D., Sharma, S., & Singh, P. (2017). Removal of methylene blue by adsorption onto activated carbon developed from Ficus carica bast. *Arabian Journal of Chemistry, 10*, S1445–S1451.
Pati, S., et al. (2021). *γ-Irradiated Chitosan From Carcinoscorpius rotundicauda (Latreille, 1802) Improves the Shelf Life of Refrigerated Aquatic Products, 8-2021*.
Putro, J. N., Santoso, S. P., Ismadji, S., & Ju, Y.-H. (2017). Investigation of heavy metal adsorption in binary system by nanocrystalline cellulose – Bentonite nanocomposite: Improvement on extended Langmuir isotherm model. *Microporous and Mesoporous Materials, 246*, 166–177.
Rabeie, B., Mahmoodi, N. M., Dargahi, A., Hayati, B., & Moghaddam, H. Rezakhani (2025). Magnetic COF/MOF hybrid: An efficient Z-scheme photocatalyst for the visible light-assisted degradation of tetracycline and malachite green. *Journal of Molecular Liquids, 421*, Article 126869.
Revellame, E. D., Fortela, D. L., Sharp, W., Hernandez, R., & Zappi, M. E. (2020). Adsorption kinetic modeling using pseudo-first order and pseudo-second order rate laws: A review. *Cleaner Engineering and Technology, 1*, Article 100032.
Souri, E., Kaboodari, A., Adib, N., & Amanlou, M. (2013). A New extractive spectrophotometric method for determination of rizatriptan dosage forms using bromocresol green. *Daru: journal of Faculty of Pharmacy, Tehran University of Medical Sciences, 21*, 12.
Subhan, F., et al. (2022). Adsorption and reusability performance of hierarchically porous silica (MMZ) for the removal of MB dye from water. *Inorganic Chemistry Communications, 139*, Article 109380.
Tamer, Y., Koşucu, A., & Berber, H. (2022). Graphene oxide incorporated chitosan/acrylamide/itaconic acid semi-interpenetrating network hydrogel bio-adsorbents for highly efficient and selective removal of cationic dyes. *International Journal of Biological Macromolecules, 219*, 273–289.
Vishwanathan, P., van Oosterhout, H., Heugens, P. P. M. A. R., Duran, P., & van Essen, M. (2020). *Strategic CSR: A Concept Building Meta-Analysis, 57*, 314–350.
Wang, B., et al. (2018). Alginate-based composites for environmental applications: A critical review. *Critical reviews in environmental science and technology, 49*, 318–356.
Wang, Y., et al. (2017). Preparation of a novel sodium alginate/polyvinyl formal composite with a double crosslinking interpenetrating network for multifunctional biomedical application. *Composites Part B: Engineering, 121*, 9–22.
Wekoye, J. N., Wanyonyi, W. C., Wangila, P. T., & Tonui, M. K. (2020). Kinetic and equilibrium studies of Congo red dye adsorption on cabbage waste powder. *Environmental Chemistry and Ecotoxicology, 2*, 24–31.
Wu, L., et al. (2019). Degradation of methylene blue by dielectric barrier discharge plasma coupled with activated carbon supported on polyurethane foam. *RSC Advances, 9*, 25967–25975.
Wu, N., Wei, H., & Zhang, L. (2012). Efficient Removal of Heavy Metal Ions with Biopolymer Template Synthesized Mesoporous Titania Beads of Hundreds of Micrometers Size. *Environmental Science & Technology, 46*, 419–425.
Yang, X., Zhang, H., Cheng, S., & Zhou, B. (2022). Optimization of the adsorption and removal of Sb(iii) by MIL-53(Fe)/GO using response surface methodology. *RSC Advances, 12*, 4101–4112.
Zhao, D., & Shen, X. (2023). *Preparation of Chitosan-Diatomite/Calcium Alginate Composite Hydrogel Beads for the Adsorption of Congo Red Dye, 15*, 2254.

Further readings

Abou Alsoaud, M. M., Taher, M. A., Hamed, A. M., Elnouby, M. S., & Omer, A. M. (2022). *Scientific Reports*.
Li, M., Wang, Z., & Li, B. (2016). Desalination and Water. *Treatment*, 16970–16980.